NSTX

TF Flex Joint and TF Bundle Stub

NSTX-CALC-132-06-00

November 23, 2009

Prepared By:

Thomas Willard

Digitally signed by Thomas Willard
DN: cn=Thomas Willard, o=PPPL, ou=Engineering, email=twillard@pppl.com, c=US
Date: 2009.11.23 16:21:15 -05'00'

Thomas Willard, PPPL Mechanical Engineering

Reviewed By:

Peter H. Titus

Digitally signed by Peter H. Titus
DN: cn=Peter H. Titus, o=Princeton Plasma Physcs Laboratory, ou=Engineering Analysis, email=ptitus@pppl.gov, c=US
Date: 2010.04.15 09:02:45 -04'00'

Peter Titus, Branch Head, Engineering Analysis Division

Reviewed By:

Phil Heitzenroeder

Digitally signed by Phil Heitzenroeder
DN: cn=Phil Heitzenroeder, o=PPPL, ou=MED, email=pheitzen@ppplgov, c=US
Date: 2010.05.04 14:45:12 -04'00'

Phil Heitzenroeder, Head, Mechanical Engineering

Table of Contents

List of Figures

List of Tables

1 Executive Summary

The objectives of this analysis of the NSTX Upgrade TF Flex Strap and TF Bundle Stub design were: 1.) to determine if the design is adequate to meet the requirements specified in the NSTX Structural Design Criteria, specifically, if the flex strap lamination stresses and the copper lead extension thread stresses meet the requirements for fatigue, yield, and buckling, under worst-case/ power supply-limit load conditions: 130,000 amps/ strap, 0.3 T poloidal field, and 1.0 T toroidal field; and 2.) to verify that the local contact pressure in the bolted electrical joints is a minimum of 1500 psi, sufficient to maintain the joint contact electrical conductance above the design goal, based on the current-design development tests, of 1.0E06 siemens/in^2.

The results of the ANSYS multiphysics finite element analysis - electric, transient thermal, magnetostatic, and static structural - show that: 1.) the maximum equivalent stress in the laminations is 27.5 ksi, which is 25.5 ksi below the fatigue allowable for the full-hard C15100 copper-zirconium strip; 2.) the maximum equivalent stress in the copper threads is 29.1 ksi, which is 32.9 ksi below the fatigue allowable for the full-hard C18150 copper-chromium-zirconium plate; 3.) the minimum average contact pressure is >6500 psi, and the minimum local contact pressure is >2500 psi, which is 1000 psi above the design goal; and 4.) the lamination minimum linear buckling load multiplier factor (LMF) is > 58, which is approximately 10x the minimum allowable specified in the NSTX Design Criteria document.

2 NSTX Upper Umbrella Assembly Upgrade Design Solid Model

The solid model of the Upper Umbrella Assembly Upgrade Design is shown in Figure 1. The design is cyclic symmetric, with twelve 3-strap TF coil segments evenly spaced around the circumference. The solid model for a Single Segment 3-Strap Assembly is shown in Figure 2

Figure 1- NSTX Upper Umbrella Assembly Upgrade Design

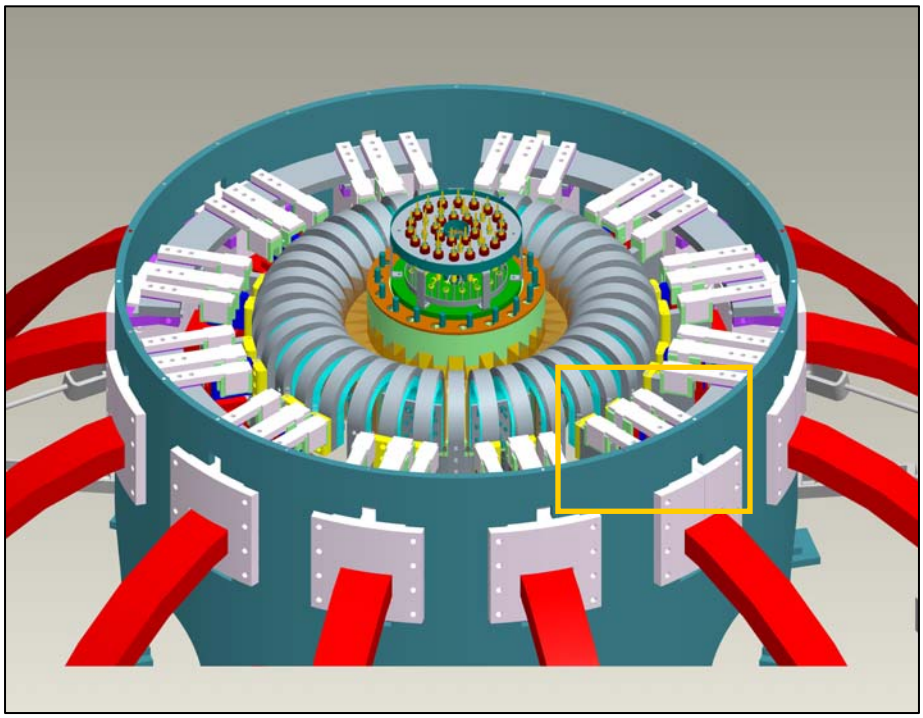

Figure 2- Single Segment 3-Strap Assembly

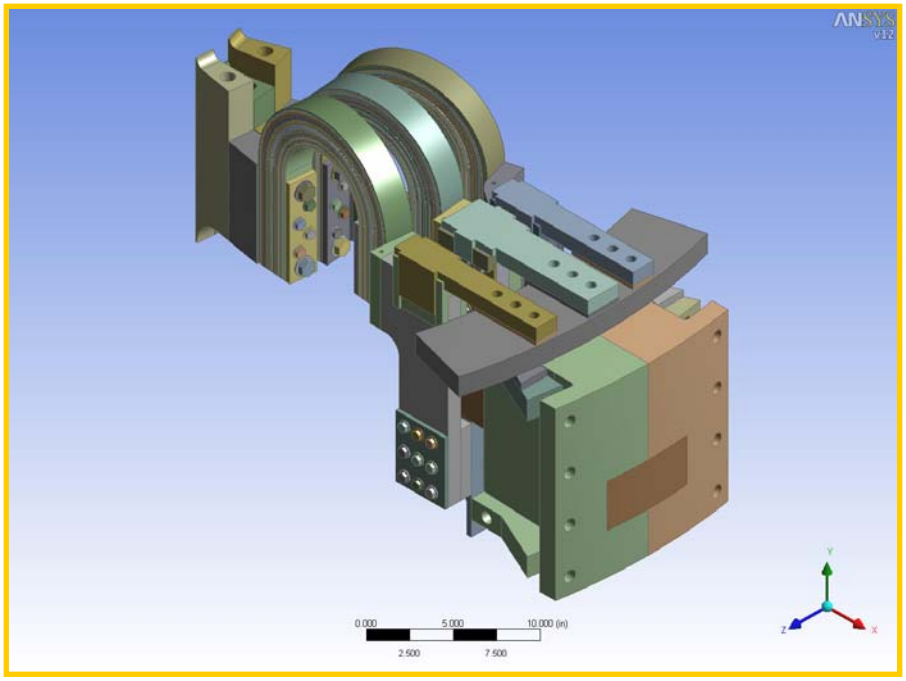

2.1 Single Strap Assembly Solid Model Description

The solid model of a Single Strap Assembly is shown in Figure 3. The strap assembly consists of an inner assembly of 19X .060" thick laminations, and an outer assembly of 12X .090" thick laminations; the gap between each lamination is .005". The material is fully-hardened C15100 H04 copper zirconium alloy, chosen for its high-temperature (>450 C) resistance to softening (see Appendix), and for its high-temperature fatigue strength (241 MPa for 300 E06 cycles).

Figure 3 - Single Strap Assembly Solid Model and Boundary Conditions

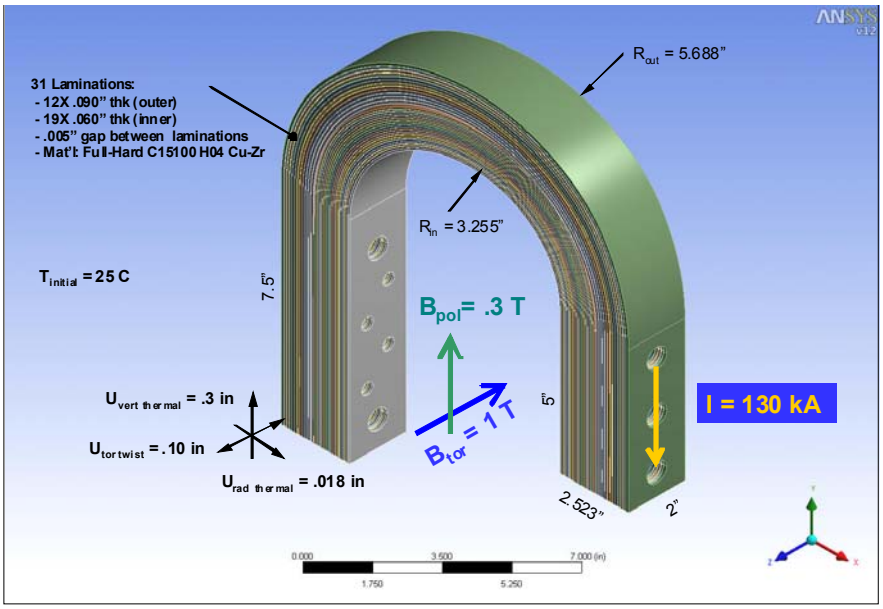

2.2 Boundary Conditions: Thermal & EM Displacements, Currents, and Applied Magnetic Fields

The boundary conditions applied to each strap assembly, for the worst-case, power supply-limit conditions, are also shown in Figure 3. Electromagnetic forces result when the total current of 130,000 kA crosses with the poloidal field of .3 T and the toroidal field of 1 T. Electromagnetic forces acting on the TF coil legs also apply a twist to the center stack (CS) relative to the vessel wall, resulting in a torsional displacement of .10". In addition to the electromagnetic forces, thermal expansion of the CS produces a .3" vertical and a .018" radial displacement of the TF Bundle Stub-end of the strap assembly, and the heat generated from high current densities produces temperature gradients, resulting in thermal strains.

3 Comparison of Current TF Joint Design versus Upgrade Design

The current TF bundle stub-end joint design is shown in Figure 4. The 12" long, C10700 silver-bearing copper TF Radial Flags are bolted to the C10700 lead extensions using four 3/8-16 Inconel 718 threaded rods, pretensioned to 5000 lbf/ea. Medium length (.562") Tap-Lok self-tapping inserts are installed in the mating face of the lead extensions.

Figure 4– Current Joint Design: TF Radial Flag

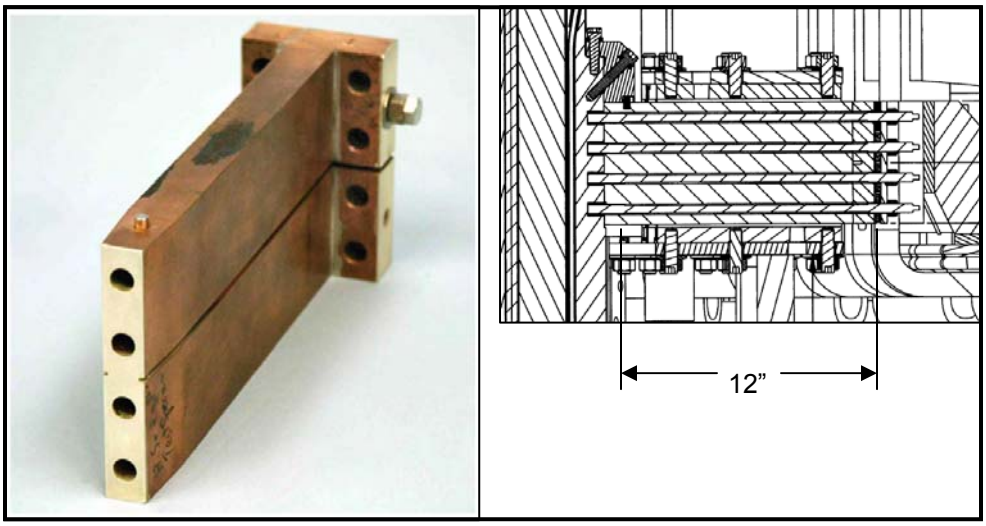

3.1 Current Joint Design Development Tests

A series of development tests were performed on the current TF joint design and included: 1.) insert cyclic pull-out tests, to determine the maximum permissible bolt pretension to prevent shear fatigue failure of the copper threads; 2.) static friction coefficient measurement of a silver-plated C10700 copper joint; and 3.) electrical contact resistance versus pressure measurements. All measurements were made at the maximum expected operating temperature of 100C.

3.1.1 Insert Cyclic Pull-Out Tests

Figure 5 shows the set-up for the insert cyclic pull-out tests. An Instron tensile test machine was used to determine the static pull-out strength as well as to establish the fatigue strength curve of the bolted joint.

The results showed that the copper threads always failed first, and that the maximum permissible bolt pretension to prevent fatigue failure within 60,000 cycles, with the additional operational cyclic load of 2000 lbf applied, was 5000 lbf.

Figure 5 - 3/8-16 Tap-Lok Insert/ C10700 Copper Thread Pull-Out Test

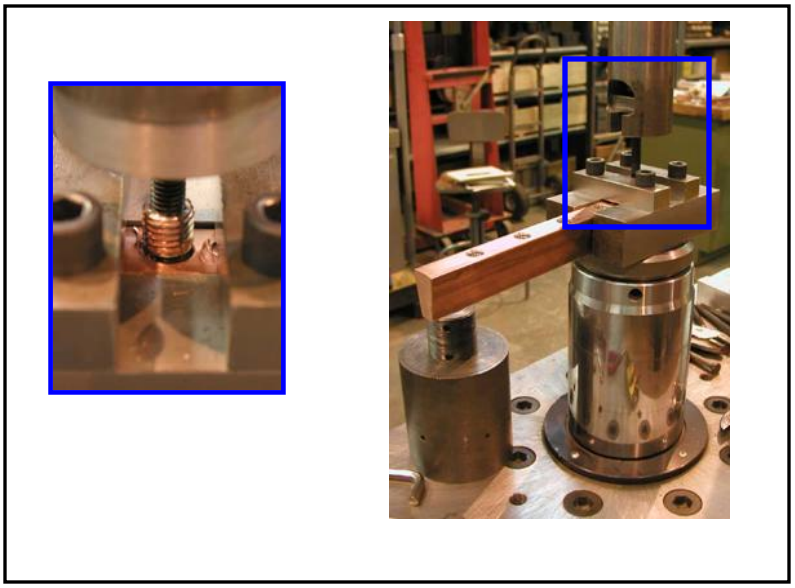

3.1.2 Static Coefficient of Friction of Silver-Plated Copper Joint

The static coefficient of friction of a silver-plated copper joint was measured using the test set-up shown in Figure 6. The Instron tensile test machine was used to apply a known lateral force to the center plate of the 3-plate stack; a load cell was used to measure the clamping force applied to the stack. The results show that the coefficient was .40, measured at the point just before sliding occurred.

Figure 6 - Static Coefficient of Friction Test

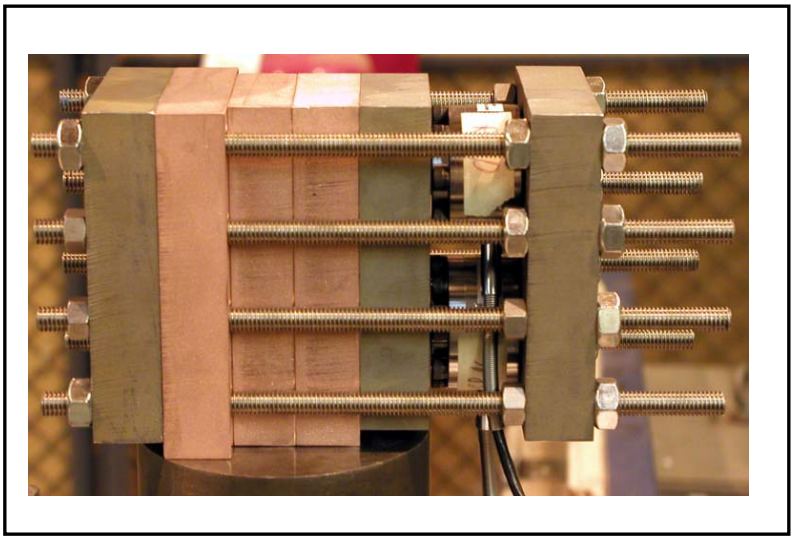

3.1.3 Electrical Contact Resistivity versus Pressure

The electrical contact resistivity versus pressure was measured using the test set-up shown in Figure 7. The Instron tensile test machine was used to apply a known axial force to the test fixture. The 100 A test current was applied using the large diameter bolts at the ends of the copper test plates. Probes on either side of the joint measured the voltage drop across the joint. The results show a sharp knee in the curve at ~1500 psi: above this pressure, the contact resistivity is a weak function of pressure. Above 4000 psi, the resistivity can be assumed to be a constant of .5 μohm m-in^2.

Figure 7 - Electrical Contact Resistivity versus Pressure

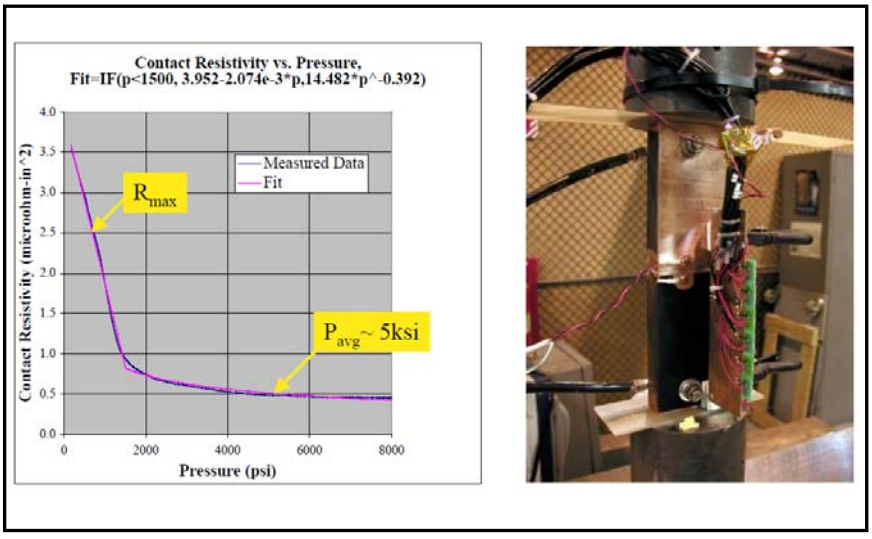

3.2 Issues with Current TF Joint Design

In-situ, operational measurements of the current-design TF joint electrical contact resistivity indicate that the joints on the levels closest to the plasma (four levels of joints: two in the top umbrella, two in the bottom umbrella) begin to separate or lift-off when the TF field strength is greater than .45 T. As the joints separate, interruption of the high current induces arcing, resulting in pitting damage on the extension-lead side of the joints. To prevent this damage from occurring over more than 25% of the joint surface, the operational TF field is limited to .55 T, instead of the design point of .6 T.

This lift-off was investigated in a separate, direct-coupled ANSYS multiphysics model of the TF Radial Flag and joint (R. Woolley, 2005), where it was shown that approximately 30% of the joint separates when the TF field strength is .6 T, as shown in Figure 7. This was later confirmed with a bench test of a bolted joint where daylight was observed between the halves of the joint when a .6 T simulated prying moment was applied to the TF Radial Flag.

Photographs of the joints, taken after 2 years of operation, show close correspondence between the observed pitting damage and the ANSYS-predicted lift-off areas (Figure 8). No pitting damage was observed in the joints on the levels furthest from the plasma, where the field strength is 1/3 the maximum value and operational voltage measurements show no signs of separation.

Figure 8 – Joint Lift-Off and Pitting Damage Areas

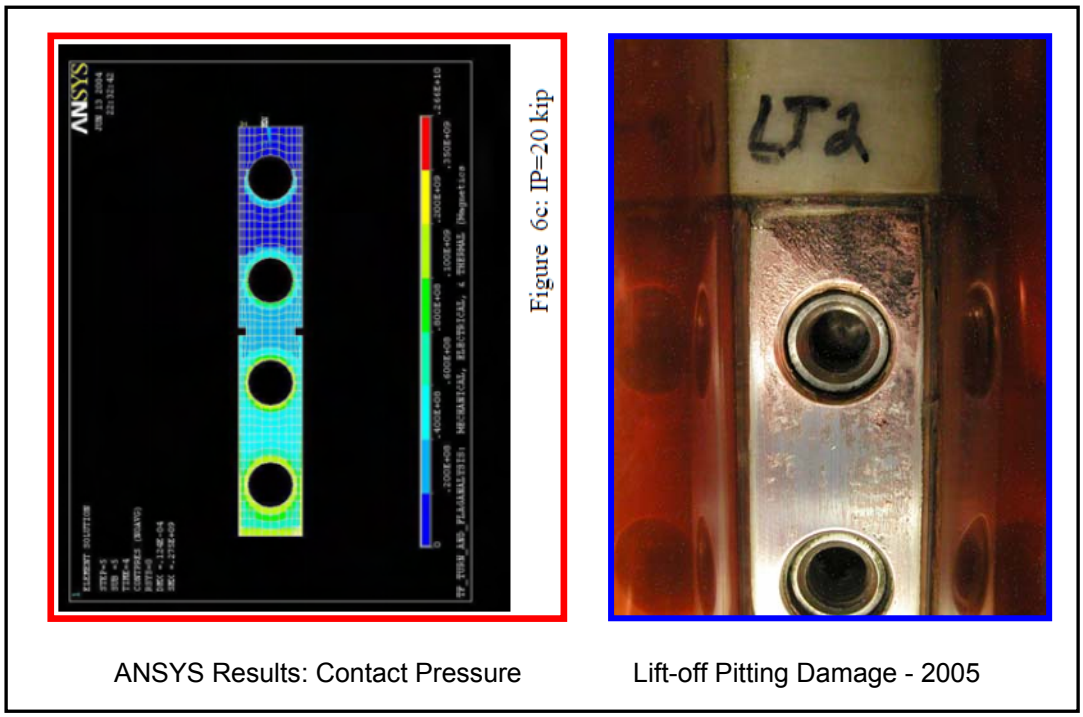

3.3 Design Operating Point Comparison

A comparison of the design operating point - TF current/ turn, TF and PF field strengths, and maximum pulse duration - for the current and upgrade designs is shown in Table 1. From the table, it is clear that the upgrade design operating point conditions are much more severe. However, it will be shown below that improvements in the upgrade design result in larger margins, even under the more severe operating conditions.

Table 1 Design Operating Point Comparison

Design	Total Current (A)	Maximum TF (Tesla)	Maximum PF (Tesla)	On-Time Pulse Duration (sec)
Current	72,000	0.8	0.1	0.5
Upgrade	130,000	1.0	0.3	7.0

3.4 Joint Mechanical Parameters Comparison

A comparison of the mechanical parameters of the TF lead-extension bolted joint designs is shown in Table 2. From the table, it is clear that the upgrade design is much more robust.

The joint is located further from the CS winding, so the joint contact area is much wider. It is also taller, so the contact area is approximately 4x larger. The number of bolts/ joint has increased, and there is a mix of 3/8 and 5/8 bolts, with the 5/8 bolts located furthest from the bolt centroid. The lead-extension material has been changed to a high strength copper alloy C18150 copper-chromium-zirconium, so that the bolt pretension is limited by the strength of the bolts and not the shear strength of the copper threads. All of this results in a nearly 5x increase in total bolt force, a 50% increase in initial contact pressure, and a large positive lift-off torque margin. Since there is no lift-off, the local contact pressure never falls below a minimum value, determined in the ANSYS analysis below to be > 2500 psi.

Table 2 Joint Mechanical Parameters Comparison

Design	Joint Contact Area (in^2)	Total Bolt Force (lbf)	Average Inlet Contact Pressure (psi)	Minimum Operating Local Contact Pressure (psi)	Calculated In-Plane Mating Torque (in-lbf)	Max TF In-Plane Mating Torque (in-lbf)	Lif-off Torque Margin
Current	3.383	20,000	5,914	0	12,500	17,500	-0.29
Upgrade	12.739	94,000	7,379	~2,500	90,875	30,143	2.01

3.5 Joint Electrical/ Thermal Parameters Comparison

A comparison of the electrical and thermal parameters of the joints is shown in Table 3. Though the total current is higher in the upgrade design, the current density is only 1/2 the density in the current design. The initial (closed joint) electrical resistance and heat generated in both designs is small, as is the estimated temperature rise across the joints, assuming no thermal capacitance.

Table 3 – Joint Electrical/Thermal Parameters Comparison

Design	Current Density (A/in^2)	Initial Electrical Resistance (W)	Heat Generated I^2 (W)	Thermal Power Density (W/in^2)	Initial Thermal Resistance (W/°C)	Zero-Heat Capacity Temperature Rise (°C)
Current	21,289	1.48E-07	7.66E+02	2.27E+02	1.18E-02	9.1
Upgrade	10,205	3.93E-08	6.63E+02	5.21E+01	3.14E-03	2.1

3.6 Static Bolt Strengths and Insert Pull-Out Loads Comparison

A comparison of the static bolt strengths and insert pull-out loads of the two joint designs is shown in Table 4. From the table, it can be seen that the shear strength of the C10700 copper threads in the current design limits the 3/8 bolt pretension to below the maximum allowable bolt load. When the estimated 2000 lbf operational cyclic load is considered, the allowable bolt pretension is reduced to only 5000 lbf: a 2000 lbf reduction due to the cyclic load, and a 3000 lbf reduction due to the reduced shear strength of the copper for fatigue at 60,000 cycles.

The upgrade design uses high strength C18150 copper-chromium-zirconium, with more than twice the shear strength of the C10700 copper, for the lead-extensions,. Also, because the extensions are longer, a longer 3/8 insert is used, with a larger shear area. This results in the copper thread strength being greater than the bolt tensile strength, so the maximum allowable bolt pretension is limited by the strength of the bolt. The bolt reactions from the ANSYS analysis below indicate that the cyclic load is small (10-15% of the bolt pretension), so can be reduced to nearly zero with the use of Belleville washers. To maximize the contact pressure and lift-off margin, without exceeding the maximum allowable bolt loads, the following bolt pretensions were chosen for the upgrade design: 10,000 lbf for the 3/8 bolts; and 27,000 lbf for the 5/8 bolts.

Table 4 Static Bolt Strength and Insert Pull-Out Load Comparison

Design	Bolt Size	Qty per Joint	Bolt Mat'l	Bolt Yield Strength (psi)	Bolt NST x D.C. Allowable (psi)	Tensile Stress Area (in^2)	Max Bolt Load	Tap-Lok Insert Outer Tread	Insert Length	Effective Shear Area (in^2)	Cu Alloy	Yield Strgth (psi)	Shear Strgth (psi)	Insert Pull-out Load (lbf)
Current	3/8-16	4	Inconel 718	186,000	138,750	0.0775	10,753	9/16-16	0.562	0.4864	C10700	36,000	20,772	10,104
Upgrade	3/8-16	4	Inconel 718	185,700	138,750	0.0775	110,753	9/16-16	0.687	0.608	C18150	75,000	43,275	26,311
	5/8-11	2				0.226	31,358	29/32-11	1.125	1.61				120,750

3.7 Comparison Summary

In summary, joint pitting damage in the current design occurs with TF fields > .45 T, in lift-off areas predicted by an ANSYS direct-coupled model and verified by in-situ measurements of joint resistivity. No pitting damage occurs in joints further from the plasma that do not lift-off. Bolt pretension, limited to 5000 lbf due to the low shear fatigue strength of the copper threads, is not sufficient to prevent lift-off, given the long lever arm of the TF Radial Flag.

The upgrade flex strap design reduces the lever arm length, minimizing the prying torque. The more robust design , with bolt pretensions limited by the strength of the bolts, also increases the mating torque, resulting in a large positive lift-off margin. A description of the ANSYS multiphysics analysis, used to determine the stresses in the laminations and the minimum local contact pressure in the joints, follows.

4 ANSYS Multiphysics Analysis

4.1 Sequential Multiphysics Model Description

The block diagram of the ANSYS multiphysics analysis used to evaluate the design is shown in Figure 9. Note: This sequential, one-way coupled model is valid only if the bolted joints do not lift-off, and if the electrical and thermal contact resistances are a weak function of pressure, which is true here if the local contact pressure is above 1500 psi.

A current of 130 kA/strap assembly was applied in an Electric analysis to determine the voltage, the current density (JS), and the Joule heating (Heat Gen) throughout the model. Next, the current density results were used in a Magnetostatic analysis, along with the toroidal field (Bz) and the poloidal field (By) strengths, to

determine the nodal Lorentz forces. In parallel, the Joule heat results were used in a Transient Thermal analysis (initial temperature T_{int} = 22 C, time duration t = 7 seconds), to determine the nodal temperatures. Finally, the Lorentz forces and temperatures were used in a Static Structural analysis, along with the displacements due to the CS thermal expansion and twist, to determine the lamination and thread stresses, and the contact status and pressure distributions on the bolted joints. A separate linear static and buckling analysis was also performed to determine the buckling load multiplier factor (LMF) of the laminations.

Figure 9 - ANSYS Multiphysics Analysis Block Diagram

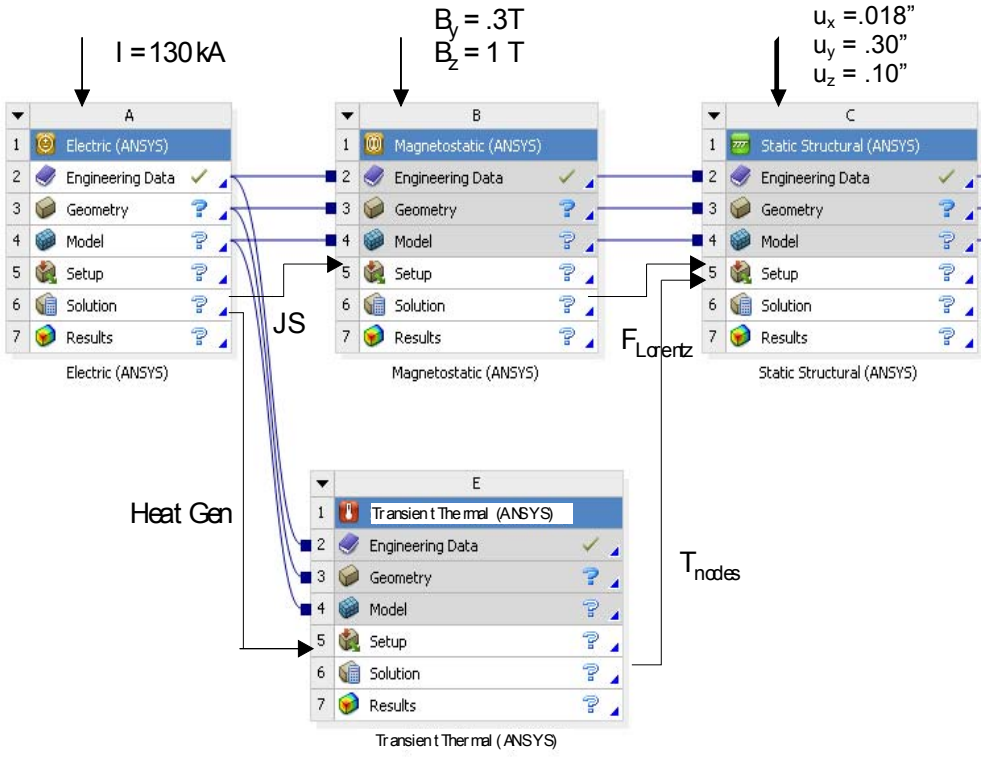

4.2 Finite Element Model Mesh

The finite element mesh of the model is shown in Figure 10. The hex-dominant mesh consists of 2,902,672 nodes and 580,846 elements. The strap laminations were meshed using the automatic thin sweep feature, with 3 divisions in the thru-thickness direction to accurately model the bending behavior.

4.3 Electric Analysis Results

4.3.1 Voltage Results

The voltage results from the Electric analysis are shown in Figure 11. The results show there is approximately a 1 volt drop across the assembly, with half the drop occurring across the strap laminations.

4.3.2 Current Density Results

The current density results from the Electric analysis are shown in Figure 12. The results show that the current through the laminations is not uniform, with the shorter, inner laminations carrying more current than the outer, even though the inner laminations are 50% thinner.

4.3.3 Joule Heat Results

The Joule heat results from the Electric analysis are shown in Figure 13. The results show that, due to the higher current densities, there is more heating of the inner laminations than the outer. The inside corners of the TF coil lead extensions, where current crowding is occurring, also experience high heat generation.

Figure 10 – Finite Element Mesh

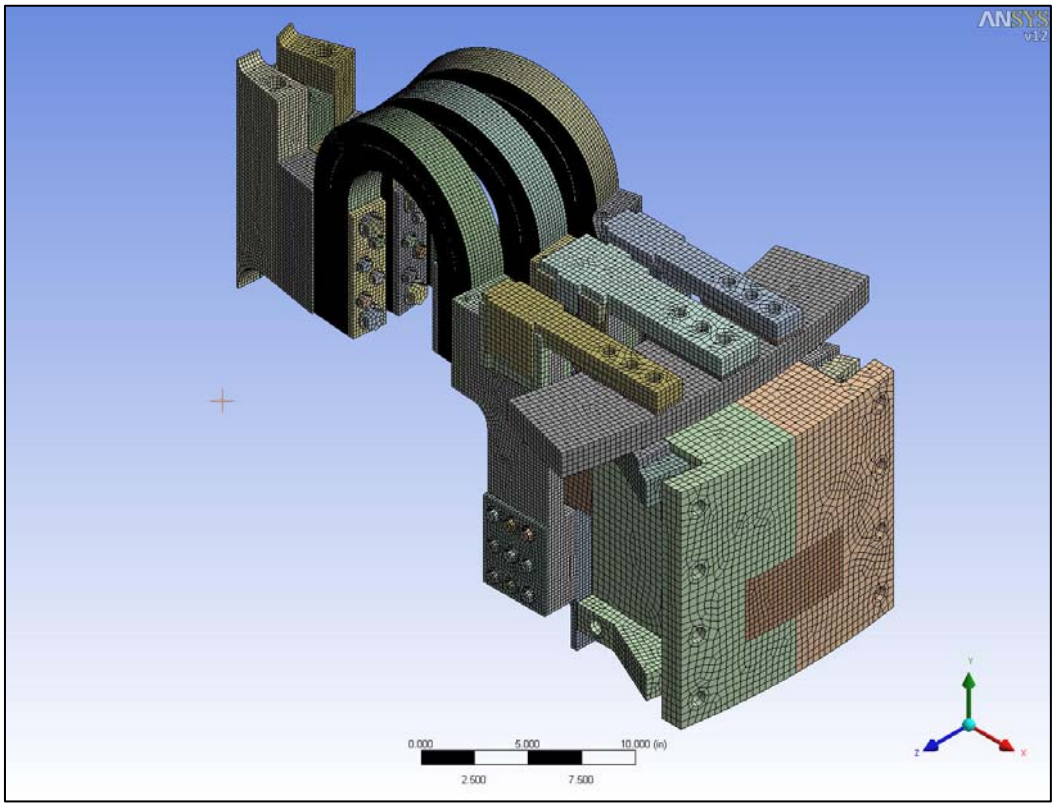

Figure 11 – Electric Analysis Results: Voltage

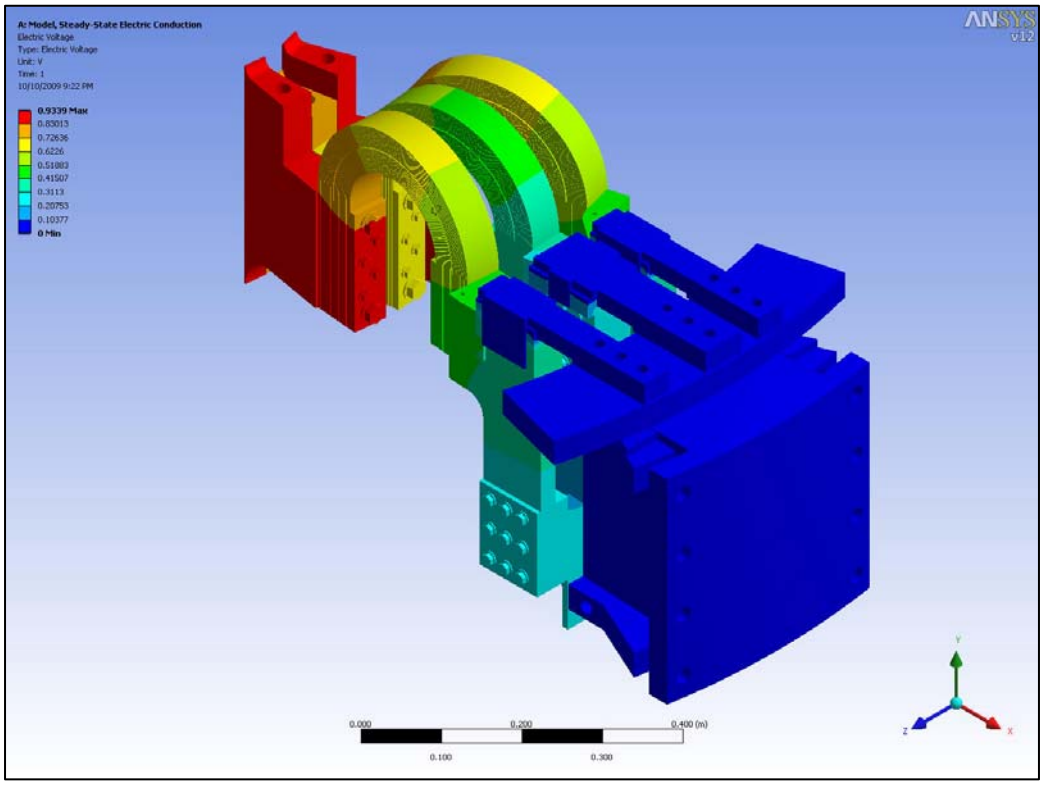

Figure 12 – Electric Analysis Results: Current Density

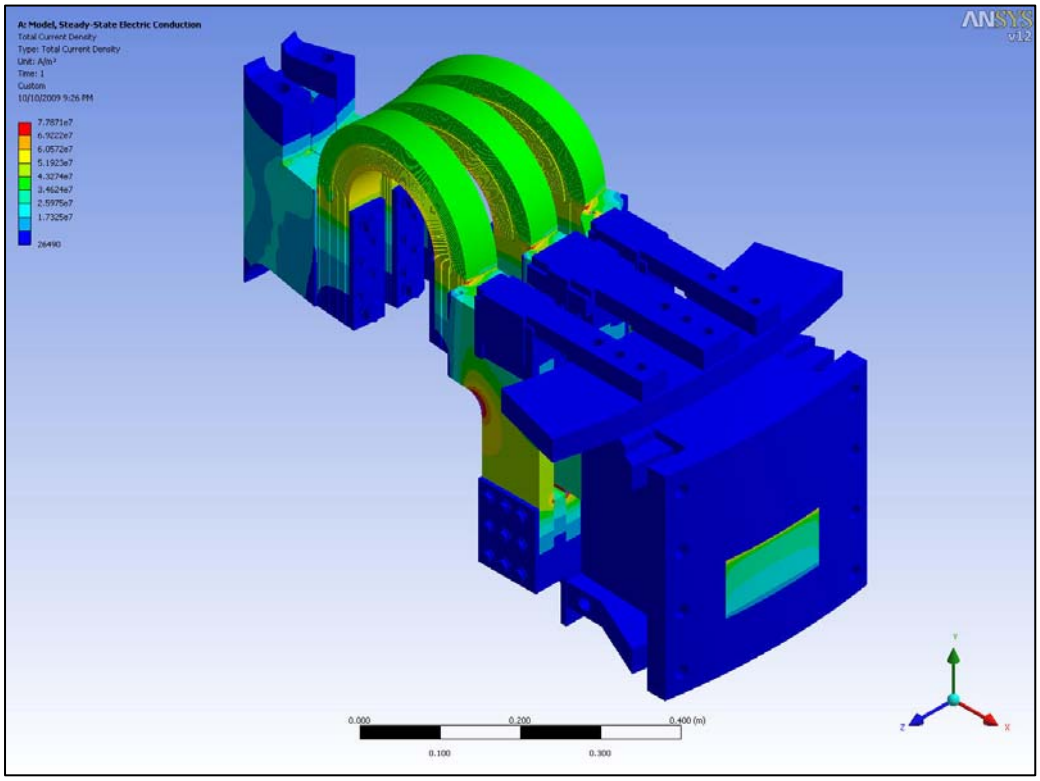

Figure 13 – Electric Analysis Results: Joule Heat

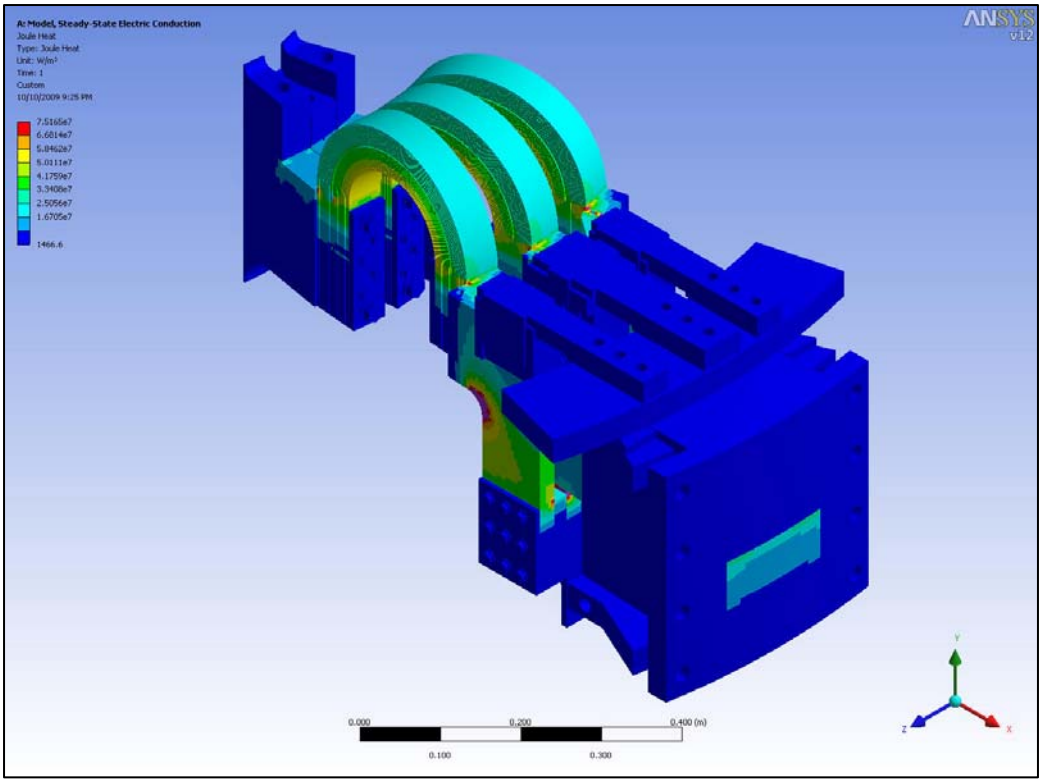

4.4 Magnetostatic Analysis Results

A vector plot of the Lorentz forces from the Magnetostatic analysis is shown in Figure 14. A close-up view of the laminations show that the forces act predominantly outward in a radial direction, resulting in a hoop stress in the laminations, but also have an out-of-plane (OOP) component, resulting in an OOP bending stress.

4.5 Transient Thermal Analysis Results

The temperature results, for time = 7 seconds, from the Transient Thermal analysis is shown in Figure 15. The results show the maximum temperature of 156 C occurs in the innermost strap lamination, where the current density is the highest, and where the heat conduction path to the 'thermal sink' of the cool, large copper plates is the longest. Significant heating also occurs in the corner radii of the TF lead extensions, where the current density and Joule heating are again high. The softening temperature of both the C15100 and C18150 copper alloys used is over 500 C, so the strength of the laminations and the lead extensions should not be affected by this heating.

4.6 Static Structural Analysis Results

4.6.1 Overall Stress Results

A plot of the von Mises stress results for the overall assembly from the Static Structural analysis is shown in Figure 16. The results show high stresses in the 304 stainless steel supports used to stabilize the tops of the TF lead extensions, as well as in the square-corner of the longest TF lead extension (close-up view). The design will be changed to eliminate these high stresses by: 1.) optimizing the shape of the supports to reduce the bending stresses, and changing the support material to Inconel 718; and 2.) adding a corner radius to the long TF lead extension.

4.6.2 Lamination Stress Results

A plot of the worst-case von Mises stress results, for both the inner and outer laminations, from the Static Structural analysis is shown in Figure 17. From the figure, the maximum stress is 27,575 psi and occurs on the outside edge of the inner lamination at the point where the lamination shape transitions from straight to curved. The maximum stress in the outer lamination is 22,171 psi and also occurs at the transition point.

Note: In a separate MathCAD analysis, not included here, it was shown that the stress in the outer laminations is dominated by the OOP bending stress due to the PF field, while the stress in the inner laminations is dominated by the in-plane bending stress due to the thermal expansion of the CS.

4.6.3 Copper Lead Extension Thread Stress Results

A plot of the von Mises stresses in the copper threaded lead extensions (outer straps) from the Static Structural analysis is show in Figure 18. Note: It wasn't possible to include enough detail in this model to accurately determine the local copper thread stresses. Instead, the average thread stress for each bolt size, based on the insert vendor's (Tap-Lok) specified effective shear areas, were used, along with the initial bolt pretensions, to determine the copper thread shear stresses. The shear stresses were then converted to the equivalent (von Mises) stresses listed in Figure 18, with the maximum of 29,047 psi occurring in the 5/8-size insert copper threads.

4.6.4 Contact Status and Pressure

Plots of contact status and pressure results for the TF lead extension joints (worst-case) from the Static Structural analysis are shown in Figure 19. The results show that no lift-off occurs in the joints, and that the minimum local contact pressure is 2500 psi, occurring over less than 5% of the joint area: the average contact pressure in the joints is greater than 6500 psi.

Figure 14 – Magnetostatic Analysis Results: Lorentz Forces

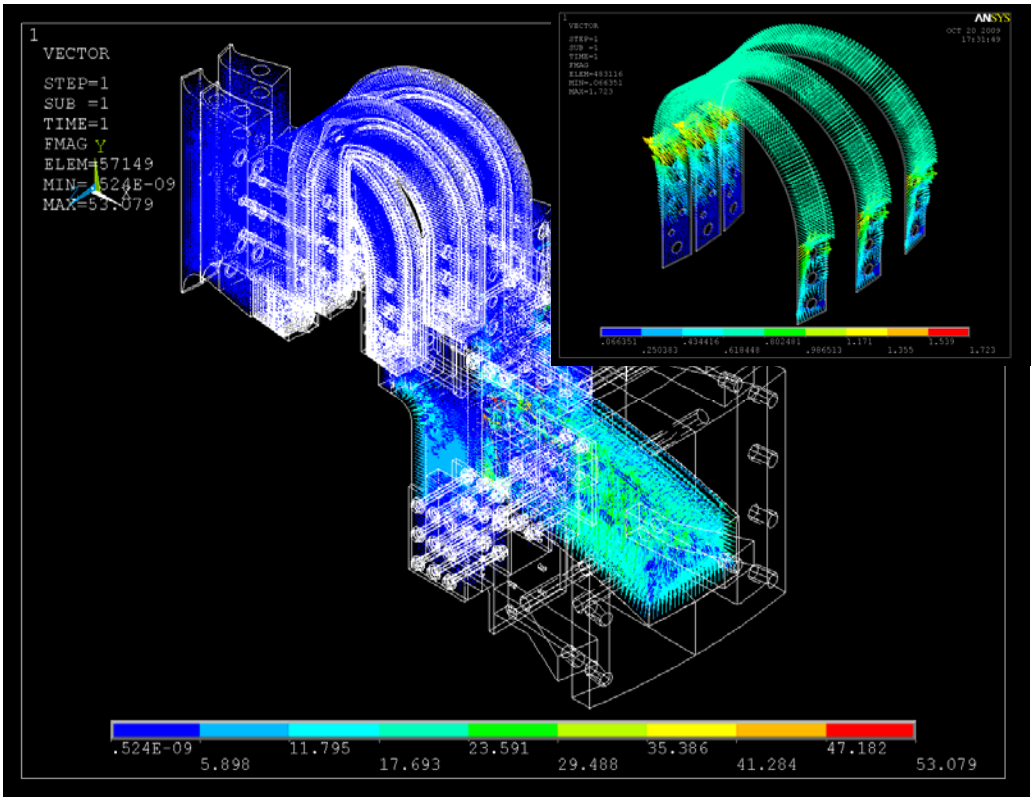

Figure 15 – Transient Thermal Analysis Results: Temperatures

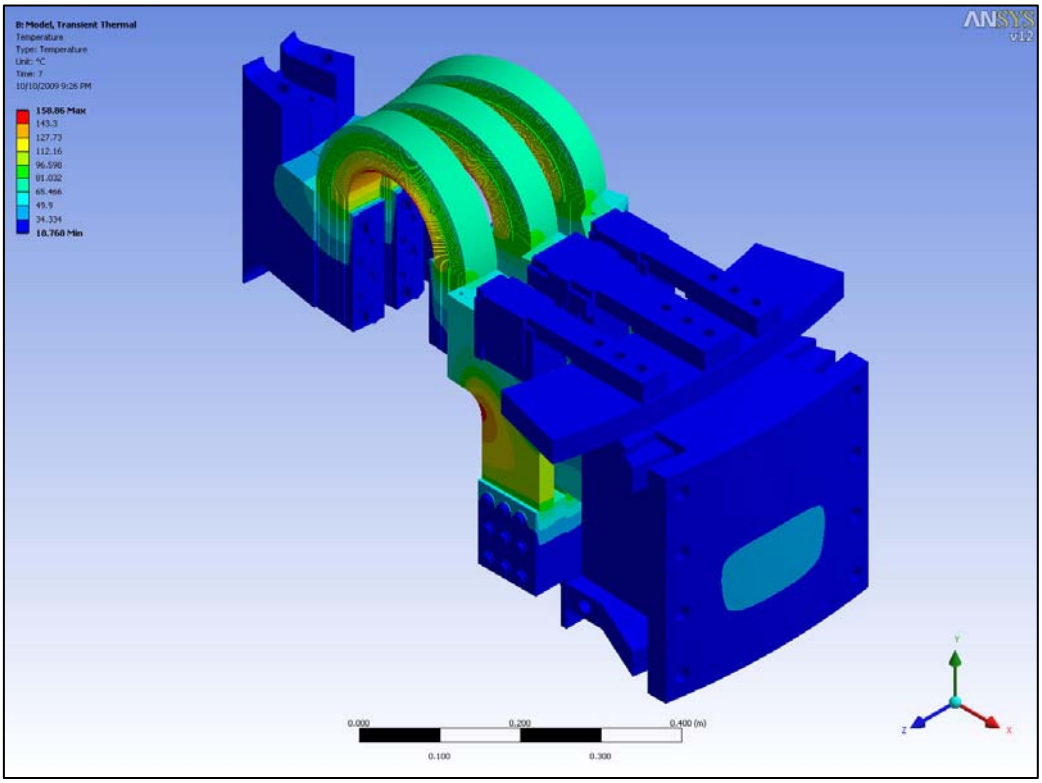

Figure 16 – Static Structural Analysis Results: von Mises Stress: Overall

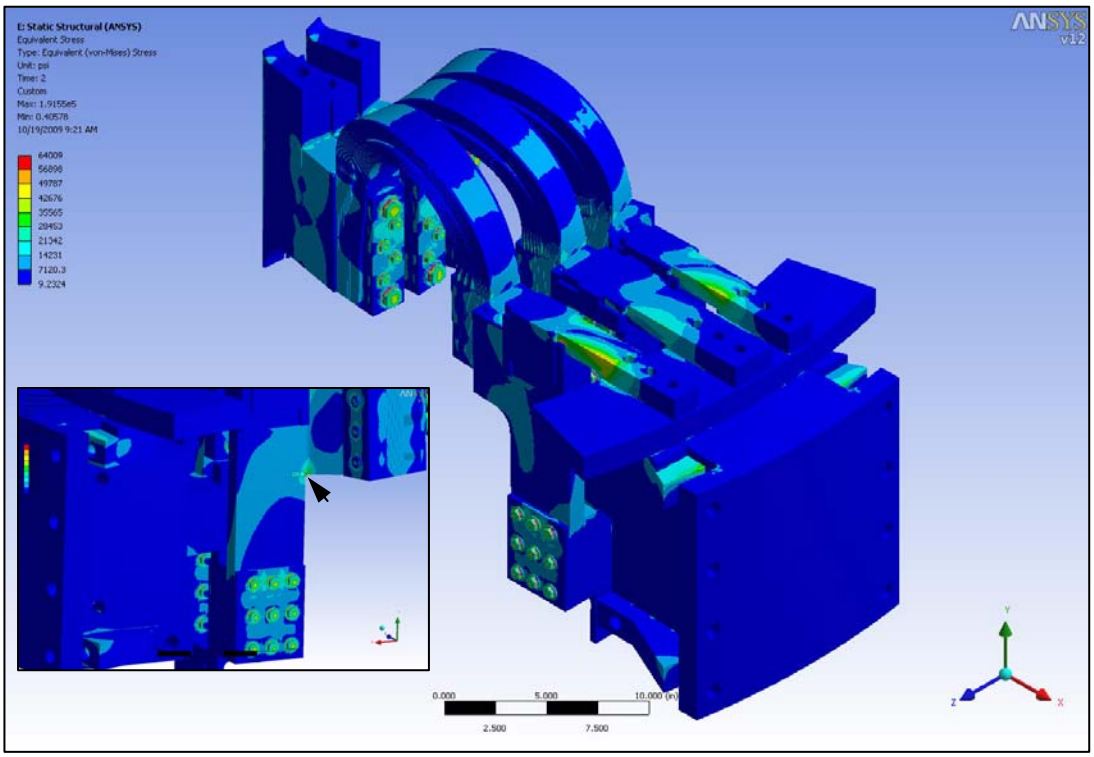

Figure 17 – Static Structural Analysis Results: von Mises Stress: Laminations

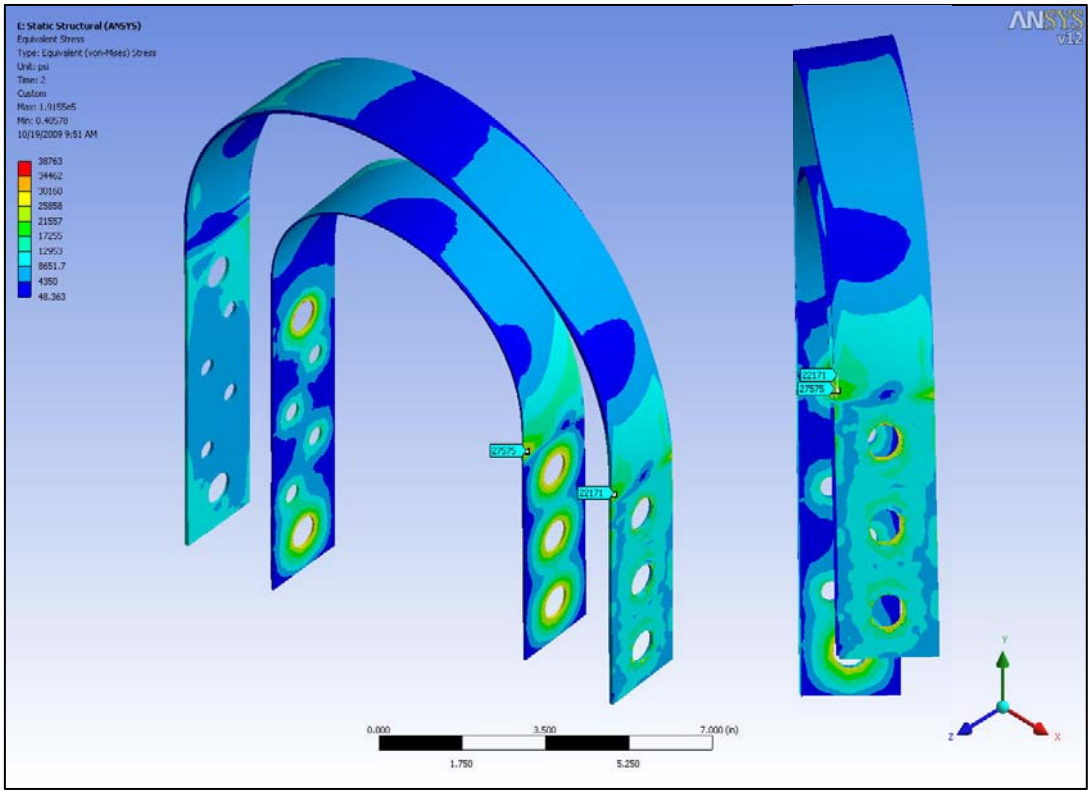

Figure 18 – Static Structural Analysis Results: von Mises Stress: Threads

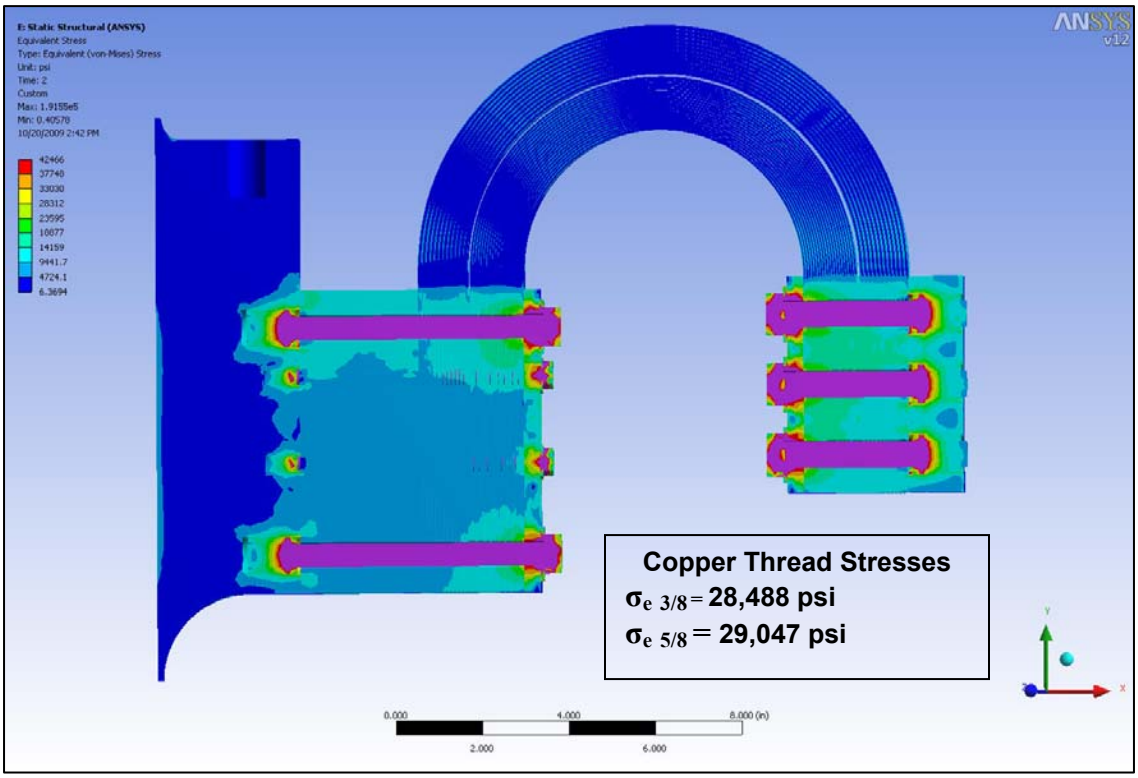

Figure 19 – Static Structural Analysis Results: TF Bundle Stub Bolted Joint Contact Pressure

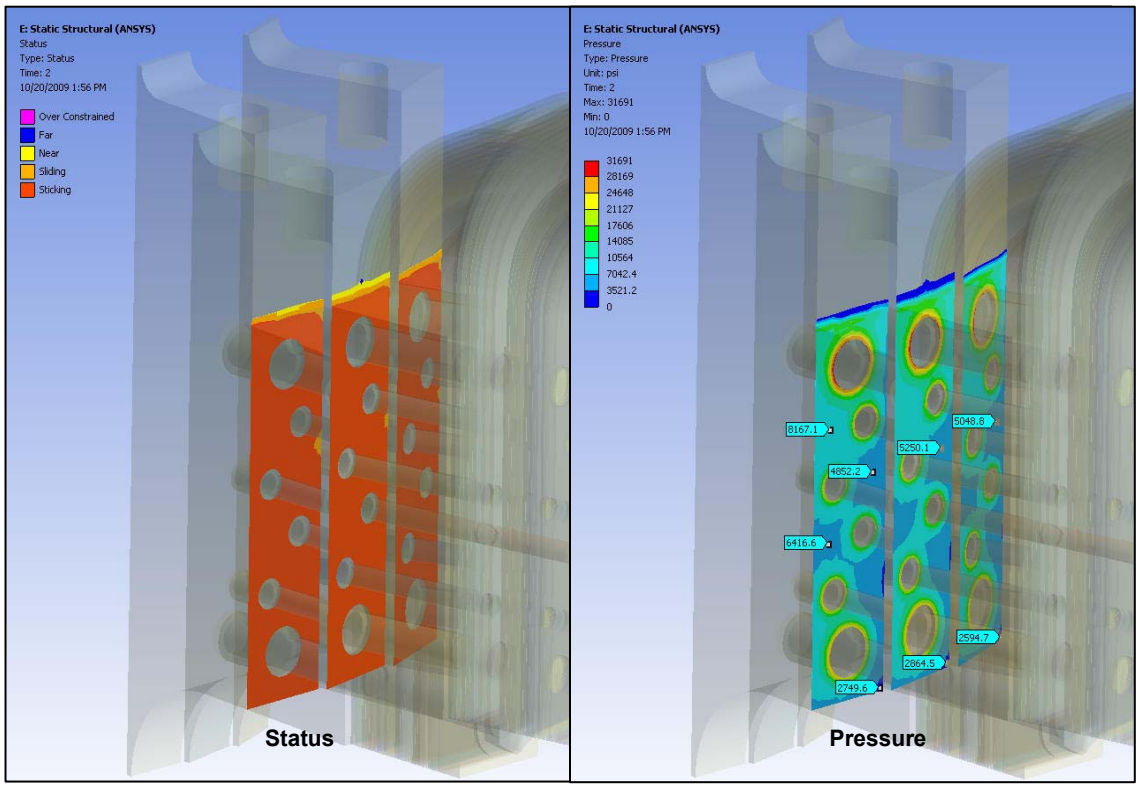

4.7 Linear Buckling Analysis Results

The results of the Linear Buckling analysis for the outer-most lamination are shown in Figure 20. The results show that buckling occurs in the same straight-to-curved transition area as where the stresses were shown to be the highest. The first-mode load multiplier factor (LMF), or scaling factor applied to all the static structural analysis lamination loads required to produce buckling, is 58.4. This value is so much greater than the margin in yield or ultimate strength of the laminations that mechanical failure will occur well before buckling.

Figure 20 – Linear Buckling Analysis Results: Load Multiplication Factor (LMF)

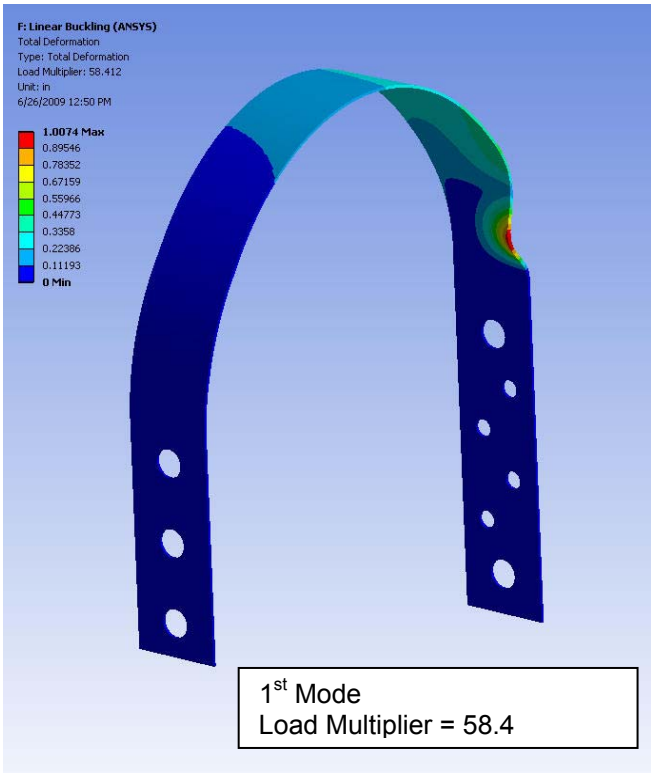

5 Conclusions

From Figure 17, the maximum equivalent (von Mises) stress in the laminations is 27.5 ksi. To satisfy the requirements of the NSTX Structural Design Criteria, the fatigue strength at 3000 cycles must be greater than twice this stress (factor of safety = 2), or the fatigue strength at 60000 cycles (20x N) must be equal to or greater than this stress, whichever is the more severe requirement. Figure 21 shows the estimated fatigue S-N curve for C15100 copper-zirconium, including plots of full power and 2/3 full power stresses at N = 3000 cycles, and N = 60000 cycles. With the factor of safety of 2 applied, the design stress level at full power slightly exceeds the fatigue strength at 3000 cycles. Because this stress was determined under worst-case power supply fault conditions, considered an extremely rare event, the design stress is judged to be acceptable and to meet the requirements of the Design Criteria. A fatigue test of a single strap assembly, under simulated worst-case load conditions, is recommended to confirm this assessment.

From Figure 18, the maximum equivalent stress in the copper threads is 29.1 ksi. Figure 22 shows the estimated fatigue S-N curve for C181500 copper-chromium-zirconium, including plots of full power and 2/3 full power stresses at N = 3000 cycles, and N = 60000 cycles. From the figure, it can be seen that the design stress meets the requirements of the Design Criteria.

Reference: "Analysis of NSTX TF Voltage Measurements", R.Woolley, PPPL memo, 2005

Figure 21 – Flex Strap Lamination Fatigue Life

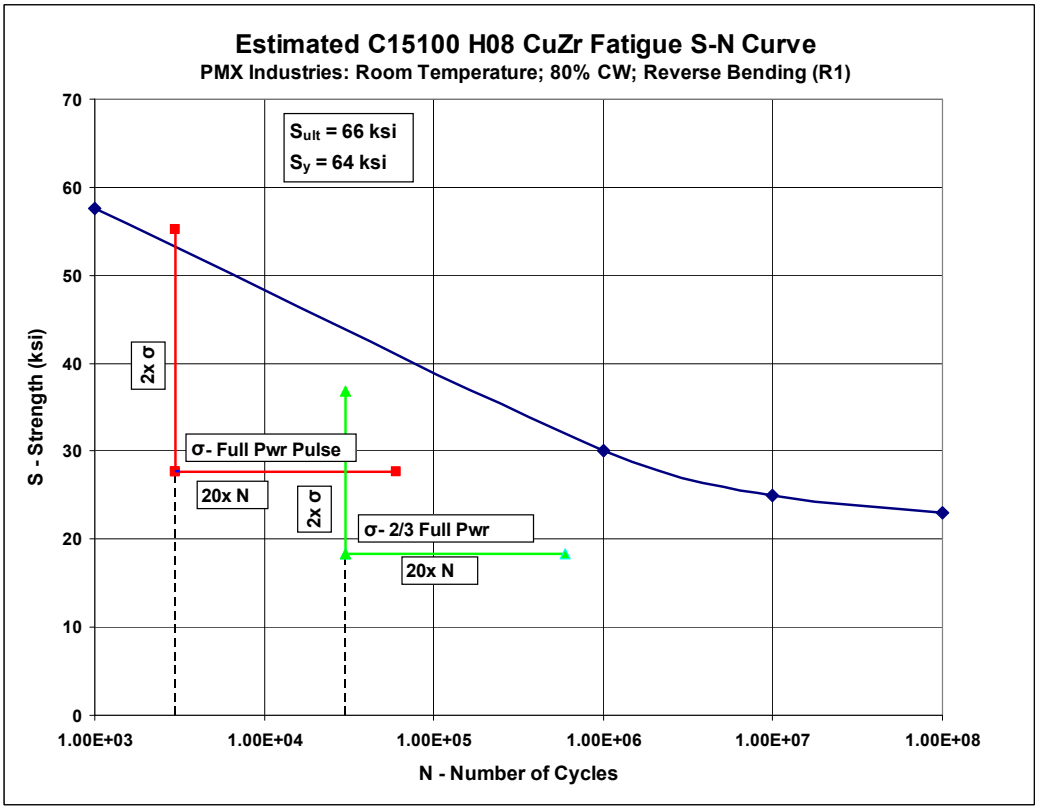

Figure 22 – Bolted Joint Copper Thread Fatigue Life

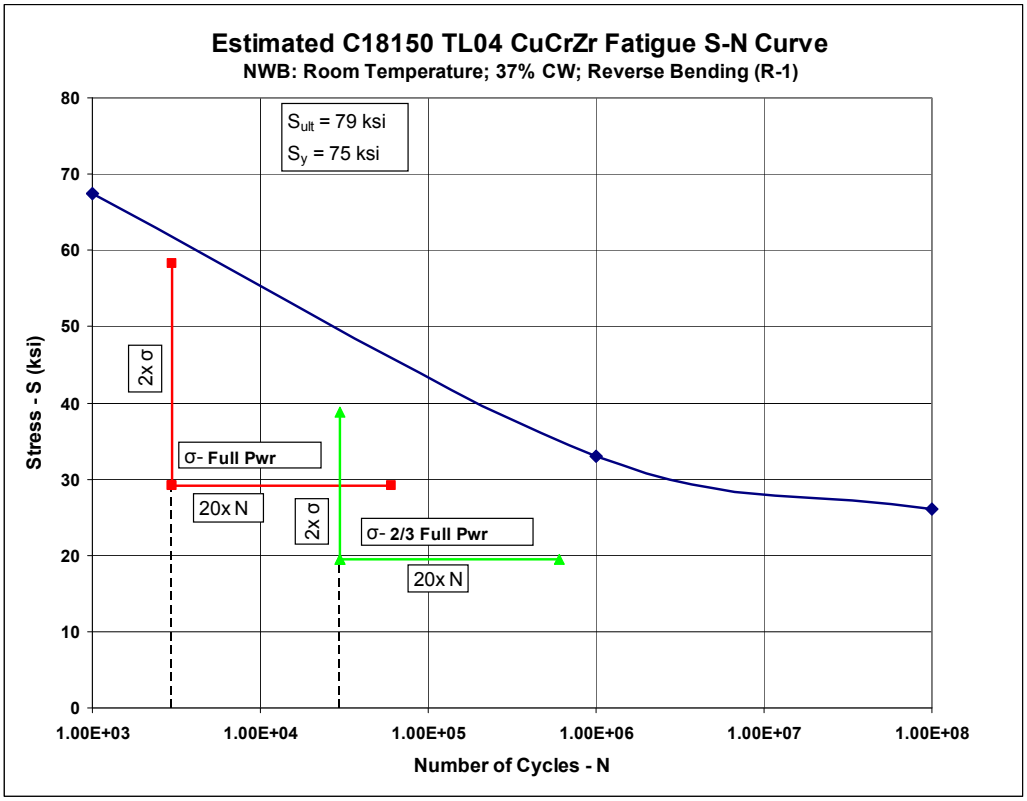

6 Appendix

Properties of some Copper Alloys

(Outokumpu Poricopper Oy)

Name	CDA	Acronym	Thermal Conductivity at 20 C [W/(m*K)]	Electrical Resistivity at 20 C [µOhm*cm]	Yield Strength Cold Worked 84% 24 C [MPa]	Yield Strength Annealed 24 C [MPa]	Fatigue Strength Cold Worked Number of Cycles[300x10^6]
Oxygen-free Copper	C10200	Cu-OF	394	1.7241-1.70	341	54.5	117
Silver-Bearing Oxygen-free Copper	C10400	Cu-OFS	394	1.74-1.71	373	-	103
Electrolytic Tough-Pitch Copper	C11000	Cu-ETP	394	1.7241-1.70	345	49.6	117
Copper-Chromium	C18200	Cu-Cr1	301-343	2.3-2.0	520	-	193
Cadmium Copper	C16200		360	1.92	474	83	205
Cupro-Nickel		Cu Ni25	33.5	34	530	140	269
Aluminum Bronze		Cu Al5	75.4-83.7	10	441	186	131
Zirconium Copper	C15000	Cu-Zr	367	1.86	414	80	241

Effect of temperature on the softening of copper alloys

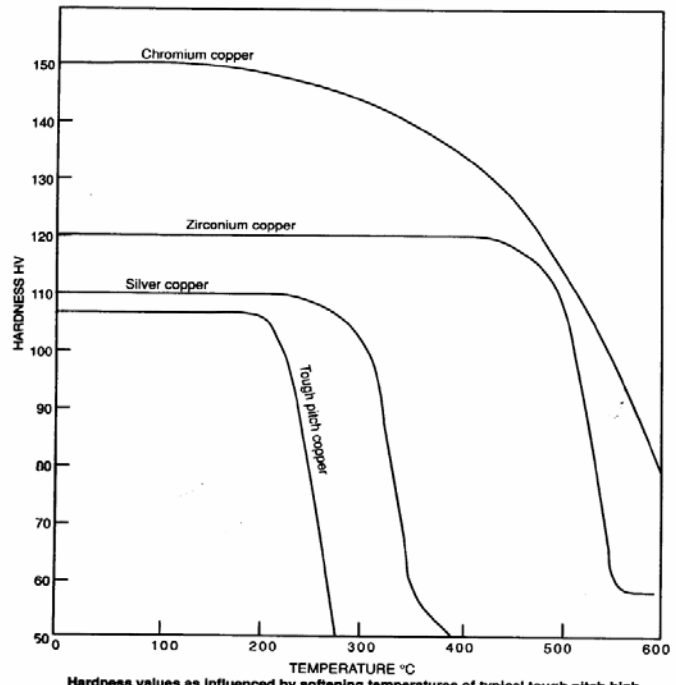

Hardness values as influenced by softening temperatures of typical tough pitch high conductivity copper, silver copper, chromium copper and zirconium copper